Equilibrium Geometry, Stability, and Magnetic Properties of Small MnO Clusters

S. K. Nayak* and P. Jena

Contribution from the Physics Department, Virginia Commonwealth University, Richmond, Virginia 23284-2000

Received May 18, 1998. Revised Manuscript Received September 18, 1998

Abstract: The equilibrium geometries, binding energies, electronic structure, and magnetic properties of small stoichiometric MnO clusters are presented for the first time. The results are based on first-principles self-consistent calculations performed within the framework of density functional theory and the generalized gradient approximation. The nature of bonding between manganese and oxygen atoms is partly ionic. The charge transfer between Mn and O atoms, as well as the average Mn−O bond distance, remains insensitive to cluster size. However, the magnetic properties of these clusters exhibit very unusual characteristics. In contrast to their bulk behavior, the small clusters of MnO are ferromagnetic with magnetic moments per MnO molecule varying between 4 and 5 μ_B. Almost all of these moments are localized at the Mn site. The $(MnO)_8$ cluster exhibits magnetic bistability, with ferromagnetic and antiferromagnetic configurations being nearly degenerate. The structural growth of these clusters also differs substantially from those of alkaline earth metal−oxide clusters in that hexagonal packing and cubic packing compete for stability. $(MnO)_2$ and $(MnO)_3$ clusters show unusual stability, making them the skeletal structures for further growth. The results agree very well with available experimental data.

Introduction

Recently, there has been considerable interest in the study of metal oxides in the bulk phase as they represent a class of technologically important materials.[1] They play major roles in high-temperature superconductivity, catalysis, corrosion, and high-temperature applications. In general, metal oxides are bonded by ionic interactions between metal and oxygen atoms, and they are insulators.[2] The presence of defects, such as oxygen, can substantially affect the electronic properties of these materials as is evidenced by the onset of high-temperature superconductivity in oxide materials.[1,2] It has been well documented that materials at the nano- or sub-nano scale possess unusual structural, electronic, optical, and magnetic properties that are very different from their behavior in the bulk phase and that these properties can be easily modified by changing the size and structure of the particles.[3] The critical length scales where novel electronic, magnetic, and optical properties manifest, however, depend on the property.[4] It is, therefore, surprising that little attention has been paid to an understanding of oxide materials at reduced sizes and in low dimensions.

Experiments on clusters and nanoparticles of metal oxides are few and far between.[5−11] It is only recently that some attention has been paid to studying the stability of oxide clusters.[10−14] While clusters of silicon oxide,[14] antimony oxide,[12] and magnesium oxide[10] having the same stoichiometric composition as in the bulk phase exhibit marked stability, transition metal oxides behave entirely differently.[10] For example, Ziemann and Castleman[10] found that $(MnO)_x$ clusters for $x = 3, 6, 9,$ and 12 exhibit conspicuous peaks in the mass spectra, indicating that these may be unusually stable. On the other hand, $(MgO)_x$ clusters show no such behavior for these sizes. It was suggested that the $(MnO)_3$ cluster having the structure of a hexagon is the building block of larger clusters which grow as hexagonally stacked rings (see Figure la). Note that, in the bulk phase, MnO has a cubic structure[15] (see Figure lb). Under certain conditions, the authors also observed the $(MnO)_2^+$ peak to be as high as the $(MnO)_3^+$ peak, leading them to conclude that in larger clusters the $(MnO)_3$ hexagonal rings are probably joined by $(MnO)_2$ square units.

This suggestion appears to conflict with the recent experiment by Chertihin and Andrews.[16] These authors have measured the infrared spectra of laser-ablated manganese atoms interacting with dioxygen. They conclude that the $(MnO)_2$ cluster is a

* Corresponding author. Present address: Princeton Material Institute and Department of Chemistry, Princeton University, Princeton, NJ 08544.
(1) Rao, C. N. R.; Raveau, B. *Transition Metal Oxides*; CVCH Publishers: New York, 1995.
(2) Cox, P. A. *Transition Metal Oxides—An Introduction to Their Electronic Structure and Properties*; Clarendon Press: Oxford, U.K., 1992.
(3) See, e.g.: Service, R. F. *Science* **1996**, *271*, 920.
(4) Reddy, B. V.; Nayak, S. K.; Khanna, S. N.; Rao, B. K.; Jena, P. *J. Phys. Chem. A* **1998**, *102*, 1748.
(5) Boutou, V.; Lebeault, M. A.; Allouche, A. R.; Bordas, C.; Paulig, F.; Viallon, J.; Chevaleyre, J. *Phys. Rev. Lett.* **1998**, *80*, 2817.
(6) Kodama, R. H.; Makhlouf, S. A.; Berkowitz, A. E. *Phys. Rev. Lett.* **1997**, *79*, 1393.

(7) Li, J.; Wang, Y. J.; Zou, B. S.; Wu, X. C.; Lin, J. G.; Guo, L.; Li, Q. S. *Appl. Phys. Lett.* **1997**, *70*, 3047.
(8) Persson, J. L.; Anderson, M.; Holmgren, L.; Aklint, T.; Rosen, A. *Chem. Phys. Lett.* **1997**, *271*, 61.
(9) Wang, L. S.; Wu, H.; Desai, S. R. *Phys. Rev. Lett.* **1996**, *76*, 4853.
(10) Ziemann, P.; Castleman, A. W., Jr. *Phys. Rev. B* **1992**, *46*, 13480.
(11) For some of the early work on oxides, see, e.g.: Freas, R. B.; Dunlap, B. I.; Waite, B. A.; Campna, J. E. *J. Chem. Phys.* **1987**, *86*, 1276. King, F. L.; Dunlap, B. I.; Parent, D. C. *J. Chem. Phys.* **1991**, *94*, 2578.
(12) Reddy, B. V.; Jena, P. *Chem. Phys. Lett.* **1998**, *288*, 253.
(13) Veliah, S.; Xiang, K.; Pandey, R.; Recio, J. M.; Newsom, J. M. *J. Phys. Chem. B* **1998**, *102*, 1126.
(14) Harkless, J. A.; Stillinger, D. K.; Stillinger, F. H. *J. Phys. Chem.* **1996**, *100*, 1098.
(15) Wyckoff, R. W. G. *Crystal Structures*; Interscience: New York, 1964.
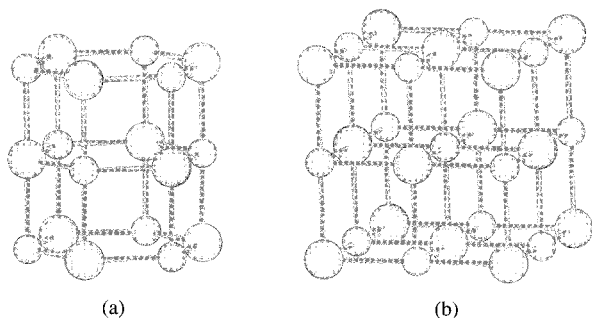(16) Chertihin, G. V.; Andrews, L. *J. Phys. Chem. A* **1997**, *101*, 8547.

Figure 1. Schematic representation of (a) hexagonal and (b) cubic structures of $(MnO)_x$ clusters. Large spheres represent Mn atoms, and small spheres represent O atoms.

rhombus with an estimated O—Mn—O angle of 101°, Mn—O bond length of 2.0 Å, and Mn—Mn bond length of 2.6 Å. The latter bond is significantly shorter than the 3.4 Å bond length of the Mn_2 dimer, suggesting significant metal—metal interaction in $(MnO)_2$.

Transition metal—oxide clusters are also expected to exhibit different electronic, magnetic, and optical properties.[2] Due to their multiple-valence structures, transition metals can form oxide clusters M_xO_y in a variety of compositions where $x \neq y$ while in the bulk phase usually $x = y = 1$.[5,8–11] Thus clusters rich in either transition metal or oxygen content can exist and, more importantly, show unusual behavior.[9] In addition, transition metal clusters, due to their d electrons, can exhibit unique magnetic properties in their oxide phases.[6,7] Recent experiments on nanoparticles of NiO[6] and MnO[7] indicate that these are ferromagnetic although in the bulk phase they order antiferromagnetically. While no experiments on the magnetic properties of free clusters of these oxides are available, ligated $Mn_{12}O_{12}$ clusters were recently found to have high spins and exhibit magnetic bistability.[17] Here four Mn^{4+} ($S = {}^3/_2$) ions form a central tetrahedron surrounded by eight Mn^{3+} ($S = 2$) ions. The spins at Mn^{4+} sites point up while the spins at Mn^{3+} sites point down. The net magnetic moment of $Mn_{12}O_{12}$ is therefore 20 μ_B.[17] No experiments on the magnetic moment of free $(MnO)_x$ clusters are available in the literature. We are also not aware of any theoretical studies of the structure and properties of free (i.e., nonligated) $(MnO)_x$ clusters, although density functional calculations on Mn—oxo and cubane complexes are available in the literature.[18]

In this paper, we present such calculations for the first time. We show that $(MnO)_3$ is indeed a magic cluster and the preferred structure is a hexagonal ring. However, we also find $(MnO)_2$ to be an equally strongly bound cluster. Its geometry is a rhombus with Mn—O and Mn—Mn bond distances in good agreement with the results of Chertihin and Andrews.[16] The most important result of our study, however, is that $(MnO)_x$ ($x \leq 9$) clusters are ferromagnetic. The moments are primarily localized at the Mn sites and vary from 5 μ_B/Mn atom in MnO to 4.1 μ_B/Mn atom in $(MnO)_9$ clusters. For $(MnO)_8$, both ferromagnetic and antiferromagnetic solutions are possible. The bonding in these clusters is partly ionic, and the Mn—Mn bond is shorter than the O—O bond. As clusters grow, two structures compete with each other for stability: cubic stacking and hexagonal stacking. For $(MnO)_6$, the cubic structure is preferred, while

for $(MnO)_9$, the hexagonal packing is preferred. Magnetically, however, these structures are very different—the magnetic moment of the cubic structure of $(MnO)_6$ is 14 μ_B larger than that of the hexagonal stacked structure, while the hexagonal-ring structure of $(MnO)_9$ has a magnetic moment 14 μ_B higher than that of the cubic structure.

Computation

Our results are based on first-principles molecular-orbital calculations using the density functional theory. The exchange-correlation contribution to the potential is treated in the generalized gradient approximation (GGA) involving both electron spin densities and their gradients using the Becke—Perdew—Wang (BPW91) prescription.[19] The geometries were optimized by calculating the forces at each atomic site and allowing the atoms to relax until the forces vanish. We have used different starting geometries for each cluster to locate not only the global equilibrium configuration but also the geometries of the isomers. These will be pointed out as we discuss each cluster separately. To ensure the accuracy of our calculations, two different basis sets along with two different computer codes (Gaussian 94[20] and DMol[21]) were used. In both codes, one solves the density functional equation for the total energy and the wave functions are taken to be antisymmetrized products of molecular orbitals. In the Gaussian 94 software,[20] the atomic orbitals are represented by the use of linear combinations of Gaussian functions. In particular, we have used 6-311G* basis functions which contain 4s3p1d/11s5p1d contracted/uncontracted Gaussians for O and 9s5p3d1f/14s9p5d1f contracted/uncontracted Gaussians for Mn. In the DMol code,[21] the basis functions are represented numerically on an atomic-centered spherical polar mesh rather than analytical functions (e.g., Gaussian functions). The angular portion of each function is given by spherical harmonics $Y_{lm}(\theta, \phi)$. The radial portion is obtained by solving the atomic density functional equation numerically. We have used double-numerical basis functions (DNP) to which a polarization function was added by solving the atomic equation for the excited state. Although both DMol and Gaussian 94 codes employed here use the same approximation for exchange and correlation contributions, the two methods have their merits and limitations. In the Gaussian 94 code, the atomic functions are fitted to Gaussian type orbitals and the accuracy of the fitting depends on the number of Gaussians used. On the other hand, the use of the Gaussian basis enables an analytical evaluation of the energy integrals, thus minimizing errors associated with numerical mesh size. In DMol, on the other hand, no errors are introduced in the fitting of the atomic functions as one uses numerical bases. But one pays the price for having to integrate matrix elements numerically. It is for these reasons that a comparison of results using the two methods can give added confidence. We should further point out that, in the DMol calculations, the energy levels of those isomers having lower symmetry were initially smeared in a self-consistent manner by 0.001 au to facilitate convergence. Once self-consistency was achieved, the total energy and optimized geometry were recalculated with the latest configuration as the starting point and without smearing the energy levels. The only exception to this rule was the $(MnO)_8$ cluster. As will be discussed in the next section, $(MnO)_8$ has three isomers which are energetically nearly degenerate. Convergence of the total energy was possible only when a small smearing (0.001 au) of the energy levels was allowed. The accuracy of the basis function is established by comparing the computed binding energy of O_2 and ionization potentials of Mn and O atoms with experiment. Using Gaussian 94 and 6-311G* basis functions, the ionization potential of Mn and O atoms are 6.89 and 13.94 eV, respectively. The corresponding values obtained from

(17) Friedman, J. R.; Sarachik, M. P.; Tajeda, J.; Ziolo, R. *Phys. Rev. Lett.* **1996**, *76*, 3830.

(18) Zhao, X. G.; Richardson, W. H.; Chien, J. L.; Li, J.; Noodlemann, L.; Tsai, H. L.; Hendrickson, D. N. *Inorg. Chem.* **1997**, *36*, 1198. Schmitt, E. A.; Noodleman, L.; Berends, E. J.; Hendrickson, D. N. *J. Am. Chem. Soc.* **1992**, *114*, 6109.

(19) Becke, A. D. *Phys. Rev. A* **1988**, *38*, 3098. Perdew, J. P.; Wang, Y. *Phys. Rev. B* **1992**, *45*, 13244. Other forms of the exchange-correlation functional such as B3LYP are also available in the literature. In an earlier paper,[34] we reported studies of Mn_2^+ using both BPW91 and B3LYP and the results were in good agreement with each other. Our experience has been that, in clusters that are well bound, the two forms of exchange correlation provide similar results.

(20) Frisch, M. J.; et al. *Gaussian 94*, Revision B.1; Gaussian Inc.: Pittsburgh, PA, 1995.

(21) *DMol Code*; Biosym Technologies, Inc.: San Diego, CA, 1995.

Table 1: Comparison between Binding Energies, E_b, Interatomic Distances, R_e, Magnetic Moment, μ, and Mulliken Charges, Z, in the MnO Cluster Obtained Using Gaussian 94 and DMol Codes

$$E_b = E(\text{Mn}) + E(\text{O}) - E(\text{MnO})$$

	Gaussian 94	DMol	expt
E_b, eV	4.25	5.65	3.83 ± 0.08
R_e, Å	1.65	1.65	1.65
$Z(\text{Mn})$	0.65	0.69	
$Z(\text{O})$	-0.65	-0.69	
$\mu(\text{Mn})$, μ_B	4.66	4.66	
$\mu(\text{O})$, μ_B	0.34	0.34	
$\mu(\text{total})$, μ_B	5.0	5.0	5.0

DMol calculations are 7.08 and 13.6 eV. These results agree well with the experimental results of 7.43 eV for the Mn atom and 13.62 eV for the O atom.[22] Both levels of theory predict the ground state of MnO to be a sextet in accordance with the available experimental data for MnO.[23] The binding energy and bond length of the O_2 molecule obtained using the Gaussian 94 code are 2.97 eV/atom and 1.22 Å, respectively. The corresponding values obtained using DMol are 2.56 eV/atom and 1.21 Å in comparison with the experimental values of 2.56 eV/atom and 1.21 Å.

Results

In the following, we discuss the equilibrium geometries, the average interatomic distances, the charge distributions, the binding energies, and the magnetic moments corresponding to the ground states and low-lying isomers of $(\text{MnO})_x$ clusters. The binding energy per MnO molecule is determined as the energy needed to dissociate the cluster into individual atoms, namely

$$E_b^x = E(\text{Mn}) + E(\text{O}) - E((\text{MnO})_x)/x \tag{1}$$

To determine the relative stability of the clusters, it is often more meaningful to compare the energy difference, ΔE, between $(\text{MnO})_x$ and the preceding cluster, $(\text{MnO})_{x-1}$, namely

$$\Delta E = E((\text{MnO})_{x-1}) - E((\text{MnO})_x) \tag{2}$$

Note that $E((\text{MnO})_x)$, $E(\text{Mn})$, and $E(\text{O})$ are the total energies of the $(\text{MnO})_x$ cluster, Mn atom, and O atom, respectively. The sign convention is such that a positive energy corresponds to energy gain. The average interatomic distance $\bar{R}_e$ between Mn and O atoms in $(\text{MnO})_x$ clusters was calculated by taking an average over all Mn−O bonds. In a similar vein, the average Mulliken charges on the Mn and O atoms were also calculated. We discuss these properties individually.

(a) MnO. In Table 1 we compare the interatomic distances, $\bar{R}_e$, binding energies, E_b, magnetic moments, μ, and charges, Z, on each of the atoms in MnO obtained using both the Gaussian 94 and DMol codes. While the structure of MnO is a trivial one, namely, linear, its electronic configuration is fairly complicated. This arises because Mn is a transition metal atom. It has five unpaired d electrons and a closed $4s^2$ shell. The ground-state spin multiplicities of the Mn and O atoms are 6 and 3, respectively. In the MnO molecule, one has to evaluate the energies for a number of spin multiplet structures and determine the appropriate magnetic configuration of the ground state. For example, using the Gaussian 94 code, we have

(22) *Molecular Spectra and Molecular Structure*; Huber, K. P., Herzberg, G., Eds.; Van Nostrand Reinhold: New York, 1974; Vol. IV.

(23) Ryan, M. F.; Fielder, A.; Schröder, D.; Schwartz, H. *J. Am. Chem. Soc.* **1995**, *117*, 2033.
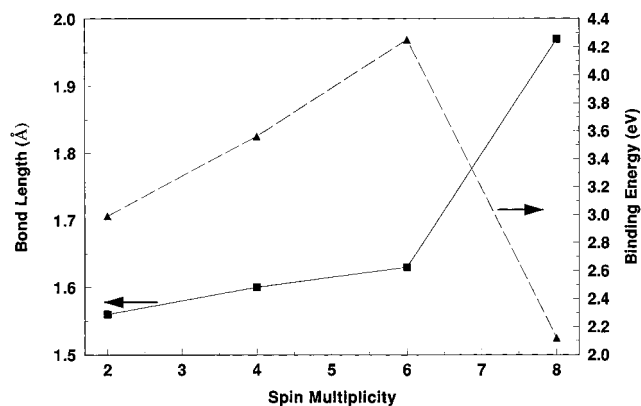
Figure 2. Bond length and binding energy of the MnO molecule for various spin multiplicities calculated using Gaussian 94 software.

calculated the total energies corresponding to spin multiplicities ($2S + 1$ where S is the spin of the cluster) of 2, 4, 6, and 8. The binding energies and bond lengths corresponding to these spin multiplicities are plotted in Figure 2. Note that the ground-state configuration corresponds to a sextet with a bond length of 1.65 Å, which compares well with the experimental bond distance of 1.65 Å in the MnO dimer.[24] The corresponding distance in bulk manganese oxide is 2.25 Å.[15] We also note from Figure 2 that the Mn−O distance increases with increasing spin multiplicity. This is to be expected, as increasing bond distance leads to decreasing overlap between atomic orbitals, which in turn gives rise to increasing magnetic moment. In the 5.0 μ_B magnetic moment of the MnO molecule, more than 90% is localized at the Mn site. The bonding between Mn and O is strong, namely 4.25 eV, and it is partly ionic in character. This is evidenced by a net charge transfer of 0.65 e from the Mn to the O atom.

The results using the DMol software are also listed in Table 1. Here, instead of energies evaluated for all possible spin multiplicities, the preferred spin multiplicities determined by the Aufbau principle are given. It is gratifying to note that the ground state magnetic configuration obtained in the DMol code agrees perfectly with that obtained in the Gaussian 94 code. The charge transfer and the bond lengths calculated using both codes are also in good agreement.

In Figure 3a we plot the total density of states (top panel) as well as those arising from the Mn 4s and 3d electrons and O 2p electrons. At the Fermi energy, the states consist of hybridized Mn 4s and 3d states as well as O 2p states. The bonding, however, is dominated by the overlap between Mn 3d and O 2p states. The distribution of O 2p levels is broader compared to that of the Mn 3d electrons. The relative localization of d electrons and delocalization of p electrons can also be seen from the deformed charge density (molecular charge density minus superimposed atomic charge density) in Figure 4a. Electrons are transferred from Mn (region marked by orange) to O (region marked by blue). Note that the distribution around Mn is more localized than that around O−consistent with the density of states in Figure 3a.

(b) $(\text{MnO})_2$. The equilibrium geometry of $(\text{MnO})_2$ is given in Figure 5. The resulting binding energies, interatomic distances, Mulliken charges, and magnetic moments calculated using both Gaussian 94 and DMol codes are given in Table 2. Both DMol and Gaussian 94 codes yield the same equilibrium geometry as well as the bond distances. Unlike that suggested by Ziemann and Castleman,[10] the preferred structure of $(\text{MnO})_2$ is a rhombus with the Mn−Mn bond distance (2.56 Å) shorter

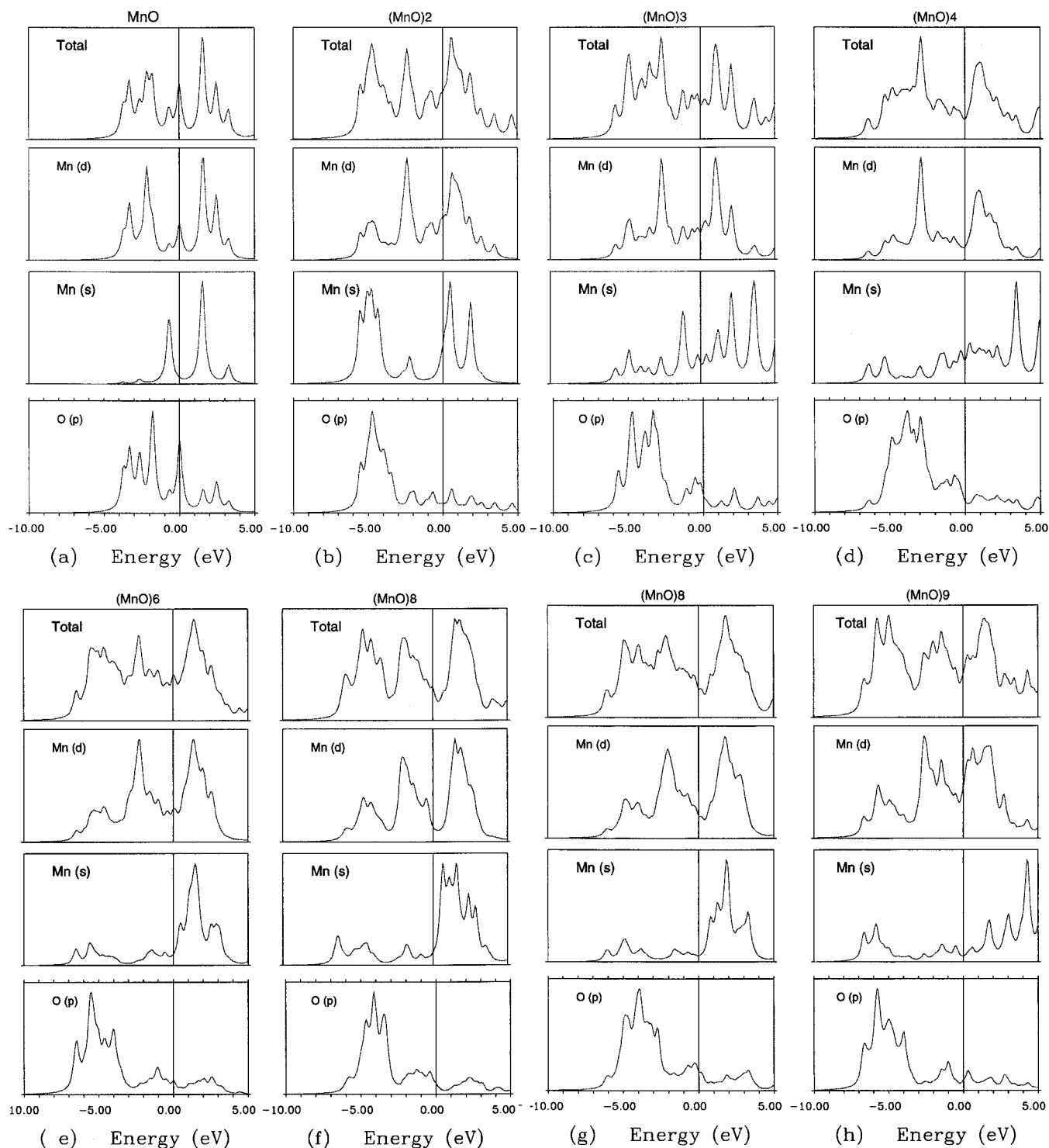(24) Bauschlicher, C. W., Jr.; Maitre, P. *Theor. Chim. Acta* **1995**, *90*, 189.

Figure 3. Total densities of states (top panels) as well as those arising from the Mn 4s and 3d electrons and the O 2p electrons (not normalized) of $(MnO)_x$ clusters corresponding to their ground state geometries. The eigenvalues are broadened with a Lorentzian by a factor of 0.2. The densities of states are given in arbitrary units. The energy scale is shifted so that the zero (vertical line) on the x axis corresponds to the highest occupied molecular orbital (HOMO) and the positive energies correspond to the unoccupied levels.

than the O—O distance (2.75 Å). It is important to note that the O—O bond in $(MnO)_2$ is broken since the bond length of the O_2 molecule is 1.21 Å. In contrast, the metal—metal bonding is enhanced since the bond length in free Mn_2 is 3.4 Å. This arises because Mn as a free atom has a half-filled d and closed s shell ($3d^5 \, 4s^2$) configuration. Thus Mn_2 is weakly bonded, and the bond strength is characterized by the van der Waals interaction.[25] In MnO, the charge transfer from Mn to O leaves the Mn atom

with a partially filled 4s shell. Thus, the two Mn atoms in $(MnO)_2$ could come closer together without suffering from Pauli repulsion. As we shall see later, this characteristic of the Mn atom remains the same as $(MnO)_x$ clusters grow in size. The contraction of the Mn—Mn bond in $(MnO)_2$ is consistent with the bond length of Mn_2^+ which has been measured in a rare-gas matrix. The removal of the electron from the antibonding s orbital of neutral Mn_2 leads to a shortening of the Mn_2^+ bond, which is 3.0 Å.

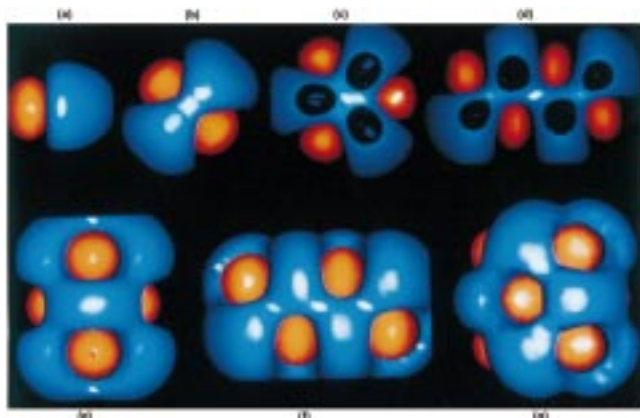(25) Morse, M. D. *Chem. Rev.* **1986**, *86*, 1049.

Figure 4. Deformed charge densities (molecular charge densities minus atomic charge densities) of $(MnO)_x$ clusters corresponding to their ground state geometries. Parts a–g correspond respectively to $x = 1$, 2, 3, 4, 6, 8, and 9. Part f corresponds to the geometry of $(MnO)_8$ in Figure 9a. The deformed density marked by orange corresponds to the region from which charge has been transferred (Mn sites) while that marked by blue corresponds to region that contains excess electrons (O sites). The open lobes arise because of the cutoff used in plotting the graph.
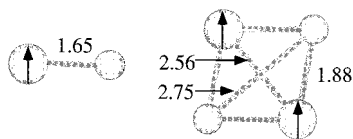

Figure 5. Equilibrium geometries of (MnO) and $(MnO)_2$ clusters. The bond lengths (Å) noted in the digrams are computed in the DMol code. The arrows indicate the direction of the magnetic moments at Mn sites.

Table 2: Comparison between Binding Energies, E_b, Interatomic Distances, R_e, Magnetic Moments, μ, and Mulliken Charges, Z, in the $(MnO)_2$ Cluster Obtained Using the Gaussian 94 and DMol Codes

$$E_b = E(Mn) + E(O) - E(MnO)_x/x$$

	Gaussian 94	DMol	expt
E_b/MnO, eV	5.88	6.91	
R_e(Mn–Mn), Å	2.34	2.56	2.60
R_e(O–O), Å	2.75	2.75	
R_e(Mn–O), Å	1.80	1.88	2.0
O–Mn–O angle, deg	99	94	100
Z(Mn)	0.81	0.75	
Z(O)	−0.81	−0.75	
μ(Mn), μ_B	3.85	3.89	
μ(O), μ_B	0.15	0.11	
μ(total), μ_B	8.0	8.0	

The Mn–O distance of 1.88 Å in $(MnO)_2$ is only slightly larger than the corresponding value of 1.65 Å in MnO. This indicates that the nature of bonding between Mn and O in $(MnO)_2$ does not change qualitatively from that in MnO. This can be further seen from the Mulliken charge transfer given in Table 2. The Mn–Mn and O–O bond distances, as well as the O–Mn–O bond angle, in Figure 2 are in good agreement with the experimental data of Chertihin and Andrews.[16]

We have repeated the above calculations using the Gaussian 94 code. As mentioned earlier, unlike in the DMol code, where the ground state spin multiplicity is determined by the Aufbau principle, in the Gaussian 94 code, one has to explicitly optimize the geometry for a specified spin multiplicity. For $(MnO)_2$, we have calculated the total energies corresponding to the equilibrium geometries with spin multiplicities ranging from 1 to 11. The preferred spin multiplicity in the Gaussian 94 code is 9,
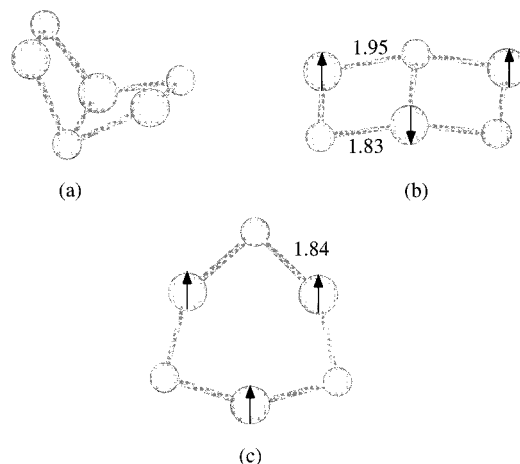

Figure 6. (a) Starting geometry of $(MnO)_3$. (b) Geometry corresponding to a metastable minimum. (c) Global equilibrium geometry. See the caption to Figure 5 for the remaining information.

which is the same as that found in the DMol code. As is the case with the MnO molecule, most of the moment (97%) is localized at the Mn sites. All the moments in $(MnO)_2$ are coupled ferromagnetically, and the total moment of $(MnO)_2$ is 8 μ_B while it is 5 μ_B in the MnO molecule.

In Figure 3b, we plot the total density of states, as well as the density of states arising due to Mn 4s and 3d electrons and O 2p electrons. The d states of Mn are broader than those in MnO cluster. The bonding between Mn and O is governed by the overlap of Mn 4s and O 2p electrons, in contrast to the behavior in MnO. However, as in the case with MnO, the width of the p states is broader than that of the Mn 3d electrons. This leads to the diffused character of the electron density associated with the p orbitals. This is reflected in the deformed charge density plotted in Figure 4b. We have used the same color scheme as that in MnO to describe the deformed density. The charge distribution around Mn sites (orange) is more localized than that around O (blue). Consequently, the magnetic character of the $(MnO)_2$ cluster is governed primarily by the Mn 3d electrons.

We now discuss the binding energies of MnO and $(MnO)_2$ as computed in both computer codes. We note that the binding energies do not agree as well as the charge transfers and the magnetic moments do. The Gaussian 94 code underestimates the binding energy of MnO by 1.40 eV and that of $(MnO)_2$ by 1.03 eV compared to those calculated in the DMol code. Since this difference is systematic, we believe that the relative stability of a $(MnO)_x$ cluster as a function of size, x, can be reliably predicted in any one of these approaches. Since computation of the preferred spin multiplicity of a cluster in the Gaussian 94 code is computer intensive, we have used the DMol software for the remainder of the calculations.

(c) $(MnO)_3$. The geometry of $(MnO)_3$ cluster was optimized by starting with a chair structure (see Figure 6a) and varying the bond lengths and angles without any symmetry constraint. The two wings of the chair quickly assumed a rhombus structure in analogy with the geometry of $(MnO)_2$, but no three-dimensional structure was found that could even exist in a metastable configuration. We obtained two planar structures where the forces at the atomic sites vanished. The threshold for these forces was set to 10^{-6} au/bohr. Figure 6b is a metastable configuration where two rhombuses are joined by a common axis. This structure lies 0.84 eV higher than the ground state structure (Figure 6c), which is a hexagon. We should remind the reader that Ziemann and Castleman[10] had suggested

Table 3: Binding Energies/MnO Molecule, E_b, Average Bond Distances, $\bar{R}_e$, Average Mulliken Charges, $\bar{Z}$, and Average Magnetic Moments, $\bar{\mu}$, at Mn and O Sites in $(MnO)_x$ Cluster Isomers

cluster	E_b/MnO, eV	$\bar{R}_e$(Mn−O), Å	$\bar{Z}$(Mn)	$\bar{Z}$(O)	$\bar{\mu}$(Mn), μ_B	$\bar{\mu}$(O), μ_B	$\bar{\mu}$(total), μ_B
$(MnO)_3$							
Figure 6b	7.50	1.89	0.77	−0.77	2.00	0.01	6.0
Figure 6c	7.83	1.84	0.77	−0.77	4.16	0.18	13.0
$(MnO)_4$							
Figure 7a	7.47	1.99	0.79	−0.79	3.88	0.12	16.0
Figure 7b	7.88	1.95	0.81	−0.81	4.73	0.27	20.0
$(MnO)_6$							
Figure 8a	7.90	1.93	0.72	−0.72	2.32	0.02	14.0
Figure 8b	8.14	2.04	0.82	−0.82	4.46	0.31	28.0
$(MnO)_8$							
Figure 9a	8.43	2.07	0.84	−0.84	4.71	0.29	40.0
Figure 9b	8.49	2.07	0.82	−0.82	0.00	0.00	0.00
Figure 9c	8.52	2.07	0.82	−0.82	0.00	0.00	0.00
$(MnO)_9$							
Figure 11a	8.45	1.93	0.74	−0.74	2.50	0.06	23.0
Figure 11b	8.61	1.99	0.79	−0.79	3.98	0.13	37.0

the structure of $(MnO)_3$ to be hexagonal. Unlike that idealized in Figure 1a, the hexagon in Figure 6c is not regular; i.e., the O−Mn−O and Mn−O−Mn angles are not 60° each. This is because the Mn−Mn distances are shorter than the O−O distances, as was found for $(MnO)_2$.

In Table 3 we list the binding energies, the average Mulliken charges on Mn and O atoms, the average Mn−O bond distances, and the magnetic moments of the $(MnO)_3$ cluster isomers. Note that, in both the structures, the amount of charge transfer is the same and most of the moments are localized at the Mn sites. However, the magnetic moment corresponding to the ground state structure is 7 μ_B larger than that of its low-lying isomer. This is partly brought about by the antiferromagnetic coupling of moments in Figure 6b. The moments at the Mn sites in Figure 6b are respectively 4.65, −3.26, and 4.65 μ_B, while those in Figure 6c are 4.16 μ_B at each of the Mn sites. The antiferromagnetic coupling between Mn atoms in Figure 6b vs ferromagnetic coupling in Figure 6c can be seen to be due to the different coordinations of Mn atoms. In Figure 6b, the two Mn atoms that are ferromagnetically aligned have 2-fold oxygen coordination while the one carrying a moment of −3.26 μ_B has 3-fold oxygen coordination. The charges on these Mn atoms are also different. The ferromagnetically coupled Mn atoms carry a charge of 0.76 while the antiferromagnetically coupled Mn atoms carry a charge of 0.79. In Figure 6c, on the other hand, all the Mn atoms are equivalent and each of them has 2-fold oxygen coordination.

In Figure 3c, we plot the total density of states (top panel) as well as those arising from the Mn 4s and 3d electrons and the O 2p electrons corresponding to the structure in Figure 6c. The electrons at the Fermi energy have hybridized Mn 4s and 3d character, and the bonding ensues due to overlap of these electrons with the O 2p states. Once again, the width of the O 2p levels is broad, contributing to the diffused character of these electrons. The deformed charge density in Figure 4c carries this signature. The localized nature of the electron distribution around Mn again illustrates the reason that most of the magnetic moments are due to the Mn 3d electrons.

(d) $(MnO)_4$. The structure of $(MnO)_4$ was optimized by allowing it to assume a three-dimensional as well as a planar configuration. For the three-dimensional structure, the optimization was carried out using D_{2d} symmetry, while for the planar structure, the symmetry constraint was C_{2h}. The resulting structures are given in Figure 7. The corresponding binding energies, average Mulliken charges, Mn−O distances, and moments at Mn and O atoms, and total magnetic moments are presented in Table 3.
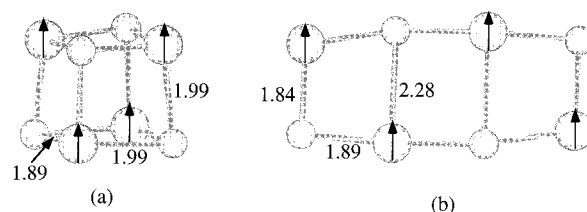

Figure 7. (a) Geometry of the metastable isomer of $(MnO)_4$. (b) Geometry of the equilibrium structure of $(MnO)_4$. See the caption of Figure 5 for the remaining information.

The distorted cubic structure lies 1.64 eV above the ground state planar structure. However, the average Mn−O bond lengths and the Mulliken charges on the atoms are nearly the same for both structures. Analogous to that of the $(MnO)_3$ cluster, the ground state of $(MnO)_4$ is more magnetic than its low-lying isomer and carries a total moment of 20 μ_B. We also note from Figure 7b that the central portion of $(MnO)_4$ is a rectangle while the outside structures are slightly distorted, namely trapezoids. We will see in the following that this is a common feature as $(MnO)_x$ clusters grow in size.

In Figure 3d we plot the total density of states as well as those arising from the Mn 4s and 3d electrons and the O 2p electrons. The Mn 3d states are narrow, and the s states are very broad. The widths of the O 2p states are also broad and overlap with the d states. The character of the electrons at the Fermi energy originates from the hybridization of the Mn d and s states. The deformed charge density plotted in Figure 4d also reveals that the charge distribution around Mn is localized while that around O is delocalized.

(e) $(MnO)_6$. This is the smallest cluster where the relative stability of hexagonal stacking versus cubic stacking can be evaluated. We optimized the geometries by constraining the cluster to have two structural forms—cubic and hexagonal as indicated in Figure 1 and subjected to C_{2h} and D_{3d} symmetries, respectively. The resulting optimized structures are given in Figure 8. The corresponding average Mulliken charges, Mn−O distances, and magnetic moments at the Mn and O sites as well as the total magnetic moments of the $(MnO)_6$ cluster isomers are presented in Table 3.

In contrast to the suggestion of Ziemann and Castleman,[10] we find the cubic-stacked structure to be lower in energy by 1.43 eV compared to the hexagonal-stacked structure. However, the average Mn−O bond distances and the average charges on the Mn and O atoms in these two structures are fairly close to each other. Interestingly, the two isomers have very different
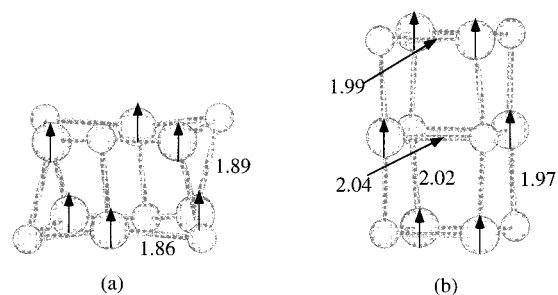
Figure 8. Equilibrium geometries of (a) hexagonal-stacked and (b) cubic-stacked structures of the $(MnO)_6$ cluster. See the caption to Figure 5 for the remaining information.

Figure 9. Equilibrium geometries of $(MnO)_8$ corresponding to (a) ferromagnetic and (b–c) antiferromagnetic configurations. See the caption to Figure 5 for the remaining information.

magnetic configurations: The lower-energy structure (cubic-stacked) has 14 μ_B more magnetic moment than the higher-energy hexagonal-stacked structure. This is consistent with our previous finding for smaller clusters; i.e., the lower-energy structure is more magnetic than the higher-energy structure. We also note from Figure 8a that the two MnO units corresponding to the top and bottom planes of the hexagon are not joined to form a squares as envisioned by Ziemann and Castleman, but are rather distorted quasi-three-dimensional units.

In Figure 3e we plot the total density of states (top panel), as well as those arising from the Mn 4s and 3d electrons and the O 2p electrons corresponding to the lower-energy structure in Figure 8b. The density of states at the Fermi energy is dominated by the Mn 3d electrons. The bonding between Mn and O results from an overlap between the Mn 3d and 4s and the O 2p electrons. As in previous clusters, the width of the O 2p states is rather broad. The deformed charge densities plotted in Figure 4e carry the characteristic signature of localized d electrons around Mn sites and delocalized p electrons around O sites.

(f) $(MnO)_8$. The structure of $(MnO)_8$ was optimized with respect to the C_2 symmetry. Unlike any other cluster we have studied thus far, $(MnO)_8$ exists in two nearly degenerate magnetic configurations: a ferromagnetic and two antiferromagnetic structures. The corresponding geometries are given in Figure 9. The binding energies, average Mn–O bond lengths, Mulliken charges, and magnetic moments at Mn and O sites are given in Table 3. We note, once again, that the bond distances and charges at atomic sites are nearly the same as those found in smaller $(MnO)_x$ clusters. What is most interesting is that the nearly degenerate isomers of $(MnO)_8$ exhibit magnetic bistability. As in previous clusters, most of the moments are localized at the Mn sites, and these moments are about 4.7 μ_B/Mn atom. The free-atomic moment of Mn is 5 μ_B. In the ferromagnetic phase, all the Mn–O bond lengths in the horizontal planes are nearly the same, namely 1.99 ± 0.03 Å. The central cubic structure is less distorted than the outer ones. This is consistent with the observation made in Figure 8b and indicates that the bulklike growth of $(MnO)_x$ clusters emerges from the clusters' center. There are two antiferromagnetic arrangements, Figure 9b,c. In Figure 9b, the magnetic moments in the left cube are aligned in the parallel direction as are the moments in the right cube. However, these two arrangements are antiparallel to each other. Note that the horizontal Mn–O bond distance (1.89 Å) in the central cube, where the coupling is antiferromagnetic, is shorter than that (1.98 Å) in the end cubes. In Figure 9c, the moments in the central cube are ferromagnetically aligned while the coupling in the end cubes is antiferromagnetic. Again, the Mn–O distance corresponding to antiferromagnetic coupling is shorter (1.89 Å) than that (1.95 Å) corresponding to ferromagnetic coupling.
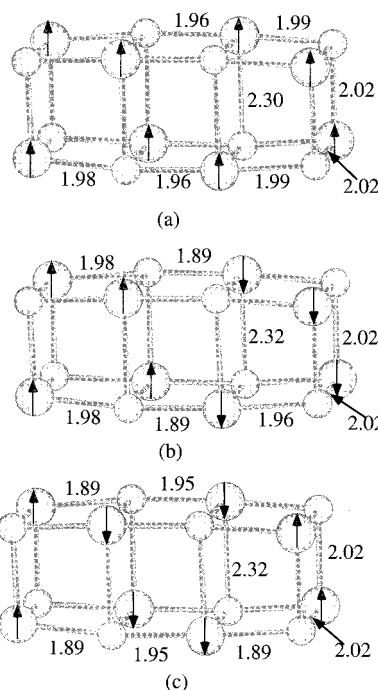
In Figure 3f,g we plot the total densities of states (top panel) as well as those arising from the Mn 4s and 3d and the O 2p electrons for the ferro- and antiferromagnetic configurations (Figure 9a,b) of $(MnO)_8$, respectively. Note that the total densities of states for the two different magnetic phases are very similar. This is also what has been found in band structure studies of ferro- and antiferromagnetic MnO crystals.[26] We also note that the s densities of states appear very similar to those in $(MnO)_4$ and $(MnO)_6$ clusters. The bonding between Mn and O again arises due to overlap between s–d hybridized Mn states and O 2p states. The deformed charge densities corresponding to the structure in Figure 9a are given in Figure 4f and provide the same consistent picture as that observed in smaller clusters. The deformed charge density distribution for antiferromagnetic solutions given in Figure 10a does not differ from that in Figure 4f.

In Figure 10b–d, we plot the spin density distributions corresponding to ferromagnetic (Figure 9a) and two antiferromagnetic (Figure 9b,c) arrangements. Here the orange color indicates spin ↑ and the blue color indicates spin ↓ distribution. Note that while, in the deformed charge density plot, Mn occupies less phase space, the opposite is true in the spin distribution plot. This is because the majority of the contribution to the moment comes from the Mn sites. We also note that the spin density distributions in Figure 10 are consistent with the Mulliken spin populations indicated in Figure 9.

The binding energies of $(MnO)_8$ having the geometries in Figure 9a–c are respectively 8.43, 8.49, and 8.52 eV per MnO unit. Within the accuracy of the calculation, these can be considered to be nearly degenerate. In bulk MnO,[27] which is antiferromagnetic, the nearest neighbor Mn atoms carry moments that are aligned in the opposite direction. In $Mn_{12}O_{12}$ acetate, on the other hand, the arrangement of the moments is ferrimagnetic where moments at the four Mn atoms constituting

(26) Towler, M. S.; Allan, N. L.; Harrison, N. M.; Saunders, V. R.; Mackrodt, W. C.; Apra, E. *Phys. Rev. B* **1994**, *50*, 5041.
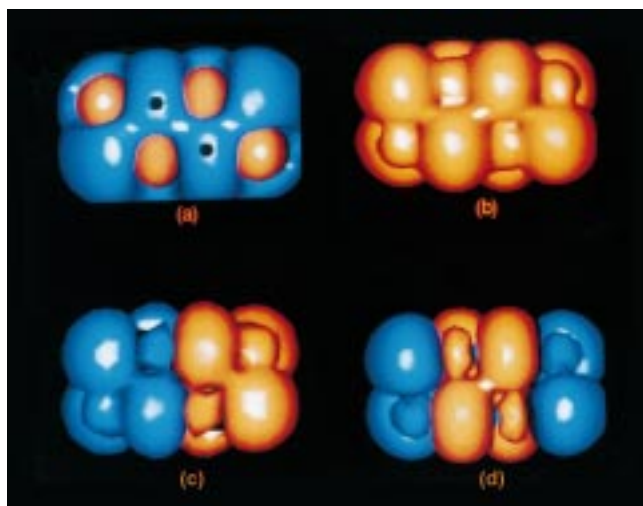(27) Cheetham, A. K.; Hope, D. A. O. *Phys. Rev. B* **1983**, *27*, 6964.

Figure 10. (a) Deformed charge density corresponding to the anti-ferromagnetic configuration in Figure 9b. (b–d) Spin density distributions for clusters in Figure 9a–c, respectively. The orange color corresponds to a spin ↑ configuration, and the blue color corresponds to a spin ↓ configuration.
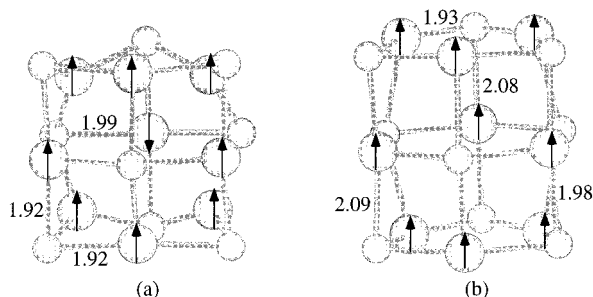

Figure 11. Equilibrium geometries of (MnO)$_9$ cluster isomers corresponding to (a) cubic-stacking and (b) hexagonal-stacking. See the caption to Figure 5 for the remaining information.

the inner tetrahedron are aligned antiparallel to the moments in the outer shell of the eight Mn atoms.[17] The evolution of the magnetic ordering described here, thus, provides a glimpse of how the ferromagnetic coupling in small clusters could change to ferrimagnetic coupling in larger clusters to antiferromagnetic coupling in the bulk.

(g) (MnO)$_9$. The geometries of (MnO)$_9$ are optimized by confining the cluster to hexagonal- and cubic-stacked structures and restricting the symmetries to D_{3h} and C_{4v}, respectively. The resulting structures are given in Figure 11. Note that in Figure 11a the cubic structure is significantly distorted and lies 1.44 eV above the hexagonal-stacked structure (Figure 11b). However, as has been the case before, these two structures are magnetically very different. Although most of the moments are localized at the Mn site, the hexagonal-stacked cluster has all the Mn moments pointed in the same direction and carries a total moment of 37 μ_B. In the cubic-stacked structure, not only is the moment at the Mn site reduced from nearly 4 μ_B/Mn to nearly 3 μ_B/Mn but also the Mn atoms in the middle plane are antiferromagnetically coupled. The total moment of the lower energy structure is 14 μ_B larger than that of its higher-energy isomer. The nature of bonding as evidenced from the Mulliken charge distribution and average Mn–O bond distance in Table 3 remains the same between the isomers. The total density of states (top panel) and those arising from Mn 4s and 3d electrons as well as O 2p electrons corresponding to the geometry in Figure 11b are given in Figure 3h. The electrons at the Fermi energy are mainly due to Mn 3d electrons, but the bonding, as
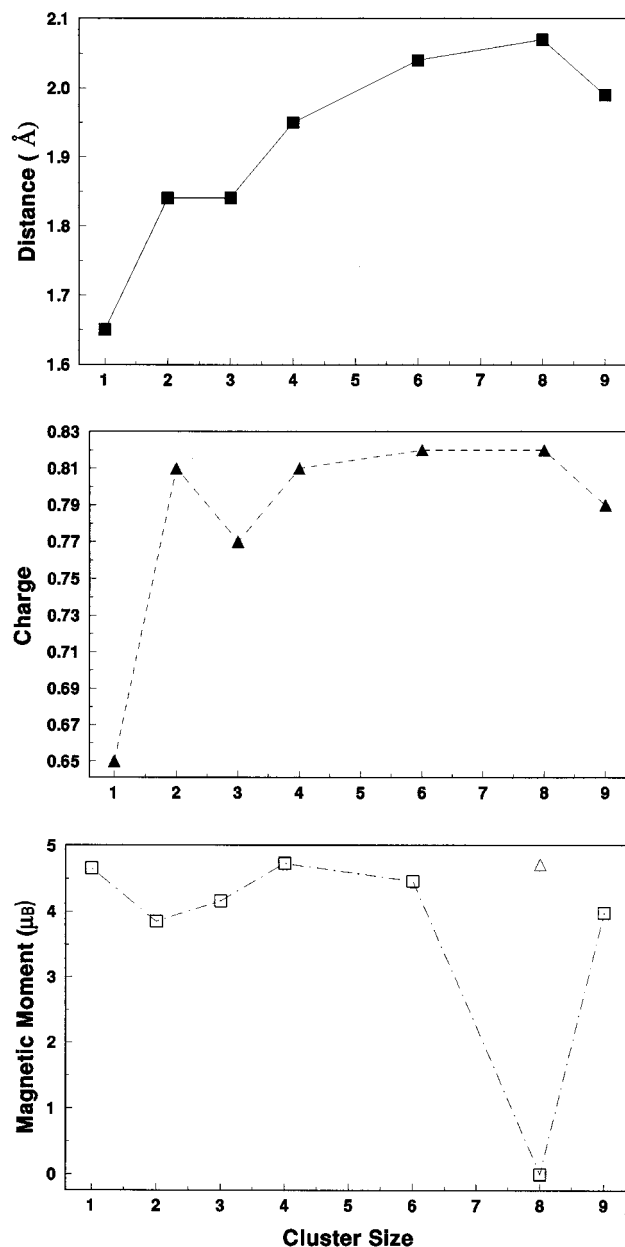

Figure 12. Average Mn–O bond distance, average charge transfer from Mn to O atoms, and magnetic moment per MnO molecule as functions of cluster size. (MnO)$_8$ has two values for the magnetic moments (see text).

in smaller clusters, arises due to overlap of Mn 4s and 3d states with O 2p states. The large width of the O 2p states is consistent with the delocalized nature of these electrons as can be clearly seen from the deformed density distribution in Figure 4g. Although there is significant p–d hybridization in the density of states, the character of the electrons near the Fermi energy is primarily d-like.

Summary

In conclusion, we present the first self-consistent calculations of the equilibrium geometries, binding energies, electronic structures, and magnetic properties of (MnO)$_x$, ($x \le 9$) clusters using the molecular orbital theory and the generalized gradient approximation to the density functional theory. The evolution of the average interatomic distance between Mn and O, the average charge transfer from Mn to O, and the magnetic moment/MnO unit is summarized in Figure 12.

Table 4: Variation of Gap between Highest Occupied Molecular Orbital (HOMO) and Lowest Unoccupied Molecular Orbital (LUMO) as a Function of Cluster Size

cluster size	HOMO−LUMO gap	cluster size	HOMO−LUMO gap
$x = 1$	1.50	$x = 6$	0.01
$x = 2$	0.28	$x = 8$	0.61
$x = 3$	0.42	$x = 9$	0.12
$x = 4$	0.56		

The HOMO−LUMO gaps as a function of cluster size are listed in Table 4. Unlike the HOMO−LUMO gaps in $(MgO)_x$ clusters,[28] which increase with decreasing cluster size, the energy gaps in $(MnO)_x$ exhibit no systematic pattern. This could arise due to the multiple oxidation states[29] of Mn and indicates that one may be able to alter the HOMO−LUMO gaps in transition metal oxides[13] by changing not only the size of the cluster but also its stoichiometric composition. The fact that $(MnO)_x$ clusters are magnetic suggests that they could have potential applications in magnetooptic devices.

The nature of bonding between Mn and O is partly ionic in all the clusters. In particular, the charge transfers from Mn to O atoms and the Mn−O bond distances are relatively insensitive to the cluster size. However, the properties of these clusters are not bulklike. In this context, MnO clusters do not behave the same as Si_xO_y, Sb_xO_y, or alkaline earth metal−oxide clusters.[10−13] They differ from their bulk behavior in many ways: (1) The equilibrium geometries are not bulklike, as there are significant distortions to the cubic structure. In addition, we find that, in some cases, hexagonal-stacked ring structures can even have lower energies than the cubic structures. (2) The Mn−O bond distances in all the $(MnO)_x$ $(x \geq 2)$ clusters studied here range between 1.9 and 2.3 Å. In manganese acetate $(Mn_{12}O_{12})$, the Mn−O distances measured by diffraction techniques range from 1.86 to 2.2 Å.[30] (3) The binding energies/MnO are particularly large for $(MnO)_x$, $x = 3, 6, 9$, and compared to other clusters. In particular, $(MnO)_4$, which could be thought of as the smallest fragment of the bulk, is bound less strongly than $(MnO)_{3,6,9}$. The energy gains in adding MnO units to the preceding $(MnO)_x$ cluster (see eq 2) are 8.16, 9.68, and 6.38 eV, respectively, for $x = 2, 3,$ and 4. This clearly establishes $(MnO)_3$ as a magic cluster and is consistent with the mass spectroscopic experiments of Ziemann and Castleman.[10] In a similar vein, the stability of $(MnO)_2$ is also comparable to that of $(MnO)_3$. (4) Larger clusters are formed either with Mn_2O_2 (rhombus) or with Mn_3O_3 (hexagon) as building blocks. In the experimentally determined structure of manganese acetate $(Mn_{12}O_{12})$, we see that the Mn_2O_2 rhombic and Mn_3O_3 hexagonal structures are also present. (5)

As cluster size increases, the energies of isomers become close to each other. Thus, it is possible that isomers with differing atomic and electronic structures can coexist. (6) The most surprising and important finding of the present work is the anomalous magnetic properties of MnO clusters. All clusters studied here carry substantial magnetic moments (4−5 μ_B per MnO unit). Most of the moments are localized at the Mn sites, and they are coupled ferromagnetically. The only exception is the $(MnO)_8$ cluster, which exhibits magnetic bistability with nearly degenerate solutions for ferromagnetic and antiferromagnetic configurations. It is important to recall that bulk MnO is antiferromagnetic and nanoparticles of MnO have been observed to be ferromagnetic. (7) The isomers of $(MnO)_x$ clusters ($x = 3, 6, 9$) exhibit strikingly different magnetic moments. The moments at O sites are usually small (∼0.3 μ_B) and are aligned ferromagnetically with Mn moments. We should point out here that Reynolds et al.[31] recently performed neutron diffraction studies on a ligated $Mn_{12}O_{12}$ cluster and found significant spin densities on oxygen and other ligand atom sites ranging from −1.0 μ_B at O sites to −0.5, 2.0, and −1.4 μ_B on various C sites. It will be interesting to study the effect of ligands on the magnetic behavior of bare clusters such as studied here.

Unfortunately, no experiments on the magnetic moments of small MnO clusters are available. However, the magnetic moment of Mn_2^+ in a rare-gas matrix has been measured to be 11 μ_B.[32] Similar experiments on Mn_5 yield the moment to be 25 μ_B.[33] Using the same level of theory as presented here, we have calculated[34] the magnetic moments of Mn clusters that agree with these experiments. We, thus, believe in the predictive capability of our theory. It is difficult to carry out measurements in small Mn clusters in the gas phase, as Mn_2, which is the seed for further growth, does not form easily because of its weak van der Waals bond. Experiments in the gas phase of $(MnO)_x$ clusters do not present this difficulty because the MnO molecule is strongly bound. In view of the prediction of ferromagnetic coupling in $(MnO)_x$ clusters made here, experiments on magnetic moments of $(MnO)_x$ clusters will be very useful. Experiments on the magnetic moments of atomic clusters have, so far, been limited to homonuclear species. We believe that compound clusters especially involving transition metal atoms, oxygen, nitrogen, and carbon will yield unexpected and novel results. We hope that this work will motivate experimentalists to begin new investigations in this area.

(28) Veliah, S.; Pandey, R.; Li, Y.; Newsam, J. M.; Vessal, B. *Chem. Phys. Lett.* **1995**, *235*, 53.

(29) Nayak, S. K.; Rao, B. K.; Khanna, S. N.; Jena, P. *J. Chem. Phys.* **1998**, *109*, 1245.

(30) Sessoli, R.; Tsai, H.; Schake, A. R.; Wang, S.; Vincent, J. B.; Folting, K.; Gatteschi, D.; Christou, G.; Hendrickson, D. N. *J. Am. Chem. Soc.* **1993**, *115*, 1804.

(31) Reynolds, P. A.; Gilbert, E. P.; Figgis, B. N. *Inorg. Chem.* **1996**, *35*, 545.

(32) Van zee, R. J.; Weltner, W., Jr. *J. Chem. Phys.* **1988**, *89*, 4444.

(33) Baumann, C. A.; Van Zee, R. J.; Bhat, S.; Weltner, W., Jr. *J. Chem. Phys.* **1983**, *78*, 190.

(34) Nayak, S. K.; Jena, P. *Chem. Phys. Lett.* **1998**, *289*, 473. Pederson, M. R.; Reuse, F.; Khanna, S. N. To be published.